Mixed positive and negative feedback loops drive diverse single-cell gene expression dynamics

Torkel E. Loman[1,2,3*], Christian P. Schwall[1*], Teresa Saez[1], Yujia Liu[1,4], James C. W. Locke[1,#]

[1]Sainsbury Laboratory, University of Cambridge, Bateman Street, Cambridge, CB2 1LR, UK

[2]Computer Science and AI Laboratory (CSAIL), Massachusetts Institute of Technology, Cambridge, US

[3]Mathematical Institute, University of Oxford, Oxford, OX2 6GG, UK

[4]Present address: Department of Biochemistry and Molecular Biology, University of Chicago, Chicago, US

*Contributed equally

[#] *Email*: james.locke@slcu.cam.ac.uk

Abstract

Genetic circuits with only a few components can generate complex gene regulatory dynamics. Here, we combine stochastic modelling and single-cell time-lapse microscopy to reveal the possible dynamics generated by a key gene circuit motif: the mixed positive/negative feedback loop. Our minimal stochastic model of this motif reveals ten distinct classes of dynamic output, including stochastic pulsing, oscillations, and bistability. These dynamics are influenced by only a few important biological parameters, such as the strength of the positive and negative feedbacks. Experimental validation in two different mixed feedback circuits in the bacterium *B. subtilis*, σ^B and σ^V, confirms our model's predictive power. Guided by our simulations, we are able to transition between dynamic behaviours by modulating *in vivo* parameters. Together, these results demonstrate how mixed feedback loops generate diverse single-cell behaviours, improving our understanding of this common biological network motif and informing our efforts to engineer them for synthetic biology applications.

Introduction

Single-cell approaches have revealed that the outputs of gene circuits can be much more heterogeneous and dynamic than previously thought. Even small circuits with a few components can generate a wide range of regulatory dynamics, including bistability (1,2), oscillations (3,4), excitability (5,6), and pulsatile activation (7,8). Stochastic effects due to low molecule numbers often play a key role in generating these dynamics (9,10). In this study, we use a combination of stochastic modelling, single-cell microscopy, and synthetic biology approaches to reveal the range of possible gene regulatory dynamics for mixed positive/negative feedback loops (a circuit type where a single component, directly or indirectly, both activates and deactivates itself, Figure 1A).

The study of mixed positive/negative feedback loops is important due to their frequent occurrence across cellular biology. Examples include circadian rhythms (11), neural signalling (12), bacterial competence (13), the cell cycle (14), and DNA damage control (15). Indeed, it has been noted that many oscillatory systems, which in principle could be produced by negative feedback loops only, also contain positive feedbacks. A potential reason is that mixed feedbacks generate more robust oscillations (16–18). Furthermore, mixed feedback loops have also been proposed as synthetic regulators in bio-engineered organisms (19).

To understand the range of gene expression dynamics possible from mixed feedback circuits, we take a stochastic modelling approach. Such techniques are often employed to capture the noisy dynamics generated by gene circuits. This noise may arise from factors like limited molecule quantities within system components (intrinsic noise) and external influences such as cell cycle phases and fluctuations in cellular energy provision (extrinsic noise). The presence of noise in gene expression has been demonstrated to play a significant role in the dynamics of numerous biological systems, and can lead to the emergence of novel and advantageous biological phenotypes. Stochastic models have been used to examine gene expression dynamics for specific cases of mixed feedback loop circuits, including for excitability in competence (13) and oscillations in circadian clocks (16). Here we formulate a minimal, stochastic, model of a mixed positive/negative feedback loop.

We use it to explore the range of dynamics possible from mixed feedback loops and how to tune *in vivo* system parameters to generate them.

To validate our model, we apply it to bacterial alternative sigma factor circuits. Alternative sigma factors direct RNA polymerase to specific downstream targets and often regulate key processes such as the general stress response, pathogenicity, and chemotaxis. The number of alternative sigma factors varies between bacterial species, ranging from 0 (as found in e.g. *Mycoplasma pneumoniae*), to over 63 (as found in *Streptomyces coelicolor*) (20–22). Alternative sigma factors are ideal model systems for studying gene regulatory dynamics, due to their well-characterised, simple, and conserved circuit structure. Furthermore, their circuits typically feature a conserved mixed positive/negative feedback loop motif, where the sigma factor activates an operon that encodes both itself and an anti-sigma factor, which antagonizes the sigma factor's activity (Figure 1B, (23–25)).

Single-cell time-lapse fluorescence microscopy has been used to study the gene expression dynamics of a range of different sigma factors. Often this has been carried out in the mother machine microfluidic device (26), which allows long-term imaging of single-cell gene expression dynamics under constant conditions (8,27). Single-cell analysis has revealed a variety of response behaviours, including stochastic pulsing (σ^B of *B. subtilis* and RpoS of *E. coli (28,29)*), a single response pulse (σ^B of *B. subtilis (30)*), and heterogeneous activation (σ^V of *B. subtilis (31)*) (Figure 1C). Here we will use σ^V as a model system for heterogeneous activation and σ^B as a model system for pulsatile gene expression dynamics.

σ^V is activated in response to lysozyme (32–34). In its inactive state, σ^V is sequestered by its anti-sigma factor RsiV. The presence of lysozyme triggers its binding to RsiV (35,36), initiating a signal transduction cascade that leads to the cleavage of RsiV and the release of σ^V (35,37,38). Freed σ^V associates with RNA polymerase, redirecting transcription toward the σ^V regulon. Notably, one of σ^V's transcriptional targets is its own operon, which includes the *sigV* and the *rsiV* gene, establishing a mixed positive/negative feedback loop. A single-cell microfluidics study has demonstrated that σ^V activation occurs heterogeneously across individual cells exposed to lysozyme stress (31).

σ^B activity is tightly controlled by its anti-sigma factor RsbW. Under stress conditions, the anti–anti-sigma factor RsbV becomes dephosphorylated, enabling it to bind RsbW. This interaction prevents RsbW from sequestering σ^B, allowing σ^B to activate its target genes, including those within its own operon, which includes RsbW, RsbV and σ^B. In addition to its role as an anti-sigma factor, RsbW exhibits kinase activity, rephosphorylating RsbV after

binding (39–41). Consequently, σ^B regulation also contains a mixed feedback loop, further complicated by partner switching between RsbW, σ^B and RsbV (42,43). Single-cell microscopy studies have revealed stochastic pulsing or single-pulse responses of σ^B, depending on the specific stress and experimental system used (28,30,44).

In this work, we develop a general mixed positive/negative feedback loop model, tracking the activity of a single component of interest. Our model describes a total of 10 distinct system behaviours, including both those that have been observed experimentally and those that have not. After non-dimensionalisation, our model is limited to six, biologically interpretable, parameters. We map how their values across parameter space determine the model's behaviour. This enables us to predict how, by tuning these six parameters, the system's behaviour can be modulated. Our model predicts distinct transitions between behaviours as the parameters *S* (self-activation strength) and *D* (self-deactivation strength) are tuned. To experimentally verify these predictions, we genetically engineered two alternative sigma factor circuits (σ^B and σ^V of *B. subtilis*) to allow us to tune these parameters. Using single-cell fluorescent microscopy to record the behaviours of the two systems, we confirmed the behavioural transitions predicted by the model. This demonstrates the ease with which mixed feedback loop circuits can be tuned to produce a variety of gene regulatory dynamics in synthetic biology applications.

Results

A general mixed positive/negative feedback loop model can reproduce experimentally observed sigma factor dynamics

To explore the range of dynamics possible from mixed feedback loop genetic circuits, we developed a minimal stochastic model (Methods, Figure 1A). In this work, we will apply it to sigma factor dynamics (a group of biologically relevant systems that features mixed feedback loops, Figure 1B). The model, a stochastic differential equation (SDE), simulates the concentration of a single component (σ). The production is modelled as a Hill function, with σ both activating and repressing its own production. The self-repression is subject to a delay (τ). In the context of sigma factors, this delay can be motivated either by the anti-sigma factor undergoing additional steps before it can interact with the sigma factor (45), or due to the presence of additional feedback mechanisms (46). Initially, our model depended on 9 parameters (Methods). Since we only wished to investigate its qualitative behaviours, we performed nondimensionalisation, reducing it to 6 parameters (Methods). They correspond

to the system's degree of self-activation (S), self-deactivation (D), the time delay in the self-deactivation (τ), base operon activity (v_0), ultrasensitivity (n), and noise amplitude (η), respectively. The deterministic version of the model (which does not feature the noise parameter η) is written as:

$$\frac{d\sigma}{dt} = v_0 + \frac{(S\cdot\sigma)^n}{(S\cdot\sigma)^n + (d\cdot\sigma(t-\tau)^n + 1} - \sigma$$

We implemented noise using the Chemical Langevin approach (CLE) (47), a well-established method for modelling noise within gene regulatory networks (48). By representing the system as a stochastic differential equation (SDE), the CLE enables fast stochastic simulations when compared to the more exact Gillespie algorithm (Gillespie, 1976; Gillespie, 1977, Supplementary Section 5.2). The CLE also allows independent tuning of the system's noise amplitude through the introduction of a system size parameter, Ω. Using an equivalent formulation, our noise term in the CLE contains the noise scaling parameter, η (where η = 0 means no noise and η = 1 means unscaled noise), and we use this to investigate the effect of noise magnitude on the system. Our results were not specific to our choice of stochastic interpretation, as we verified that implementing noise through the Gillespie algorithm generated similar results (Gillespie, 1976; Gillespie, 1977, Supplementary Section 5.2).

We implemented the delay, τ, in our simulations as a distributed delay using the linear chain trick (49,50). This enabled us to model the system as an SDE, rather than as a Stochastic Distributed Delay Equation (SDDE), which is advantageous for model simulation and analysis (Methods). However, we also provide an SDDE implementation of the model (Methods), confirming that it can replicate key results (Supplementary Section 5.1). Finally, we note that our minimal mixed feedback loop model can recreate the various sigma factor response behaviours that have been observed in the literature (Figure 1C).

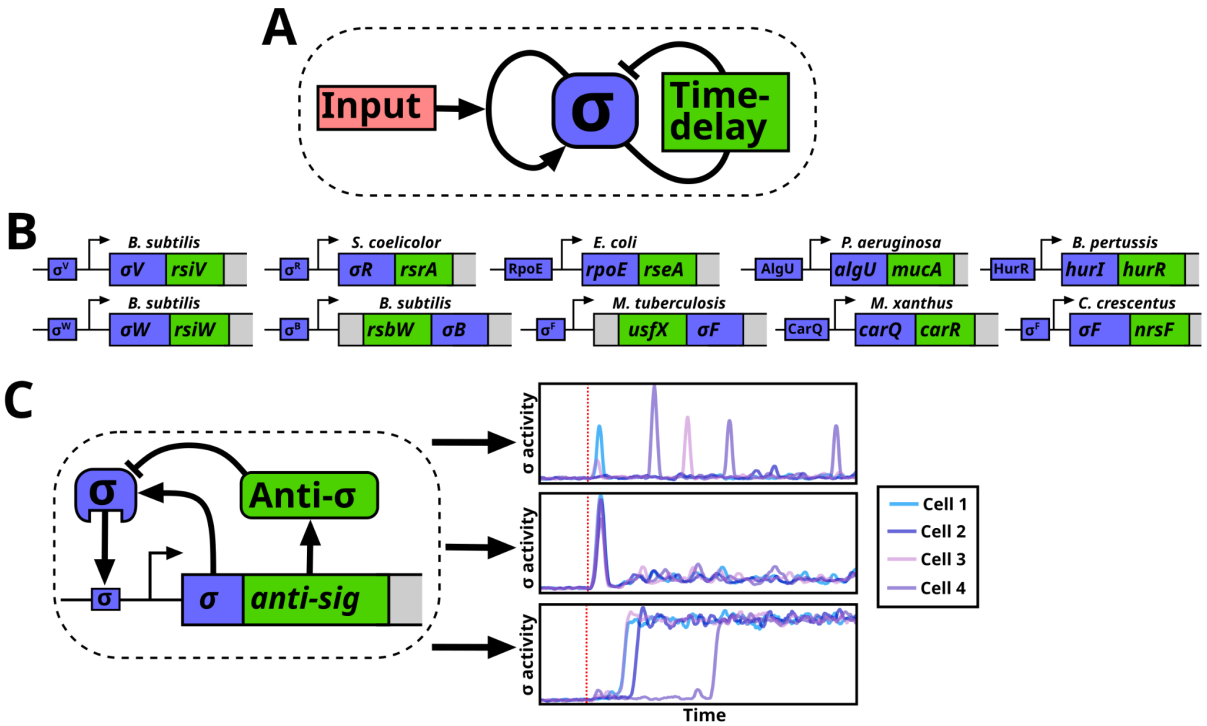

Figure 1: A general model of a mixed positive/negative feedback loop can reproduce experimentally observed sigma factor dynamics. (A) *Schematic of the general mixed positive/negative feedback loop model. Here, a single component (σ) both activates and deactivates its own production. The activation depends on the presence of an input, and the deactivation is subject to a time delay.* ***(B)*** *The mixed positive feedback loop is a common motif among alternative sigma factor circuits. Shown are simplified operon structures of alternative sigma factor circuits in a range of bacterial species, all consisting of a mixed positive/negative feedback. Anti-sigma factors (that repress sigma factor activity) are shown in green, and sigma factors are depicted in blue.* ***(C)*** *Model simulations can capture known activation behaviours, including heterogeneous activation (bottom right, as observed in e.g. σ^V (31)), stochastic pulsing (top right, as observed in e.g. σ^M (8)), and single pulse dynamics (middle right, as observed in σ^B under environmental stress (30)).*

The model can produce ten different distinct response behaviours

To explore the range of behaviours the model can exhibit and understand how these depend on its parameters, we developed a behaviour classification scheme (Supplementary Section 6.1). The scheme is based on steady state analysis, where we note that the system can have either a fixed point in an inactive state, an active state, both, or a single fixed point of intermediate activity (Supplementary Section 2). Asymptotically, it will approach one of these states, however, perturbations (either due to noise or onset of the input) can cause a transition to another state. By enumerating all possible combinations of these transitions, we defined a total of ten behavioural classes (Figure 2, Supplementary Figure 22). Simulating the model across a large set of randomised parameter values and verifying that each

simulation aligns with one of the predefined classes confirmed that these were the only robust behaviours present (Supplementary Figures 25, 26). A discussion of rarer additional behaviours, which can be considered distinct from the aforementioned ten, is provided in Supplementary Section 6.1.

Through our classification scheme, we identified ten distinct response behaviours predicted by the model (Figure 2):

1. No activity: The system remains inactive. In the absence of the input, this is also the system's default behaviour (Figure 2A, Supplementary Figure 10).
2. Stochastic pulsing: The system exhibits randomly distributed pulses of activity in time, from an otherwise inactive state (Figure 2B, Supplementary Figure 11).
3. Oscillation: The system alternates between low and high activity in a periodic manner (Figure 2C, Supplementary Figure 12).
4. Stochastic anti-pulsing: The system activates in response to the input, but displays randomly distributed pulses of inactivity over time (Figure 2D, Supplementary Figure 13).
5. Homogeneous activation: In response to the input, the system transitions from an inactive to an active state. The response times are instantaneous (and thus homogeneous across simulations) (Figure 2F, Supplementary Figure 14).
6. Heterogeneous activation: In response to the input, the system transitions from an inactive to an active state. The response times are random (and thus heterogeneous across simulations) (Figure 2E, Supplementary Figure 15).
7. Stochastic switching: The system alternates randomly between an inactive and active state (Figure 2G, Supplementary Figure 16).
8. Stable bistability: The system has an inactive and an active state, but can not switch between them intrinsically. An extrinsic way to induce such a switch would be to add additional σ from an external source (Figure 2H, Supplementary Figure 17).
9. Single response pulse: The system exhibits a single pulse of activity at the input's onset, but no significant activity thereafter (Figure 2I, Supplementary Figure 18).
10. Intermediate activation: Following input onset, the system transitions to and remains in a state of intermediate activity (Figure 2J, Supplementary Figure 19).

These behaviours include all previously observed dynamics among bacterial sigma factors (a single response pulse, stochastic pulsing, heterogeneous activation, and homogeneous activation), as well as several novel behaviours (8,28,30,31). Detailed descriptions of each behaviour are provided in the supplementary material (Supplementary Sections 4.1-4.10).

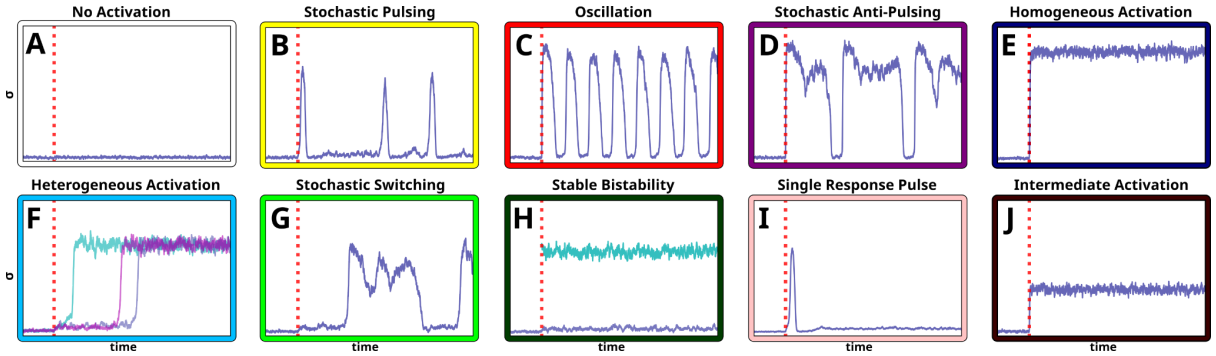

Figure 2. The model generates 10 different distinct response behaviours. *Simulations for 10 different parameter sets, demonstrating the 10 different behaviours the model can achieve. Initially, the system remains inactive; upon triggering the input (marked by the red dotted line), distinct behaviours emerge:* ***(A)*** *No activation.* ***(B)*** *Stochastic pulsing.* ***(C)*** *Oscillation.* ***(D)*** *Stochastic anti-pulsing.* ***(E)*** *Homogenous activation.* ***(F)*** *Heterogeneous activation (three different simulations displayed).* ***(G)*** *Stochastic switching.* ***(H)*** *Stable bistability. The figure depicts two simulations. The first (dark blue) is initiated at the initiative state at the same time as the simulation in the other figures. The second (turquoise) is initiated at the time of the input (dotted red line) in the active state. There is no intrinsic way for the system to switch between these two states (however, it could happen by e.g. the addition of exogenous σ).* ***(I)*** *Single response pulse.* ***(J)*** *Intermediate activation.*

The model behaviours can be mapped across parameter space

Next, we aimed to investigate how the system's properties, represented by the values of its six parameters (S, D, τ, v_0, n, and η), influence the behaviour it generates. To do this, we developed a heuristic classifier that takes a parameter set as input and assigns it to one of the 10 behavioural classes (Supplementary Section 6.3). The classifier is based on a decision tree, where each node performs simulations initialised at the model's steady states and measures the transition times to other steady states (Supplementary Figure 24). We empirically validated the classifier by verifying the accuracy of a large random sample of classifications (Supplementary Figures 25, 26). By applying the classifier across the 6d parameter space, we created a map showing which behaviour occurs for each parameter combination (Supplementary Section 3.1). By plotting 2d slices of this parameter space, with the remaining four parameters held constant, we illustrated how the system's properties (parameters) influence the behaviour it displays (Figure 3).

When examining parameter maps for various values of (τ,v_0,n,η) we found that they can be broadly divided into two regions: $D \lesssim 1$ and $D \gtrsim 1$. Each region is characterised by a distinct behavioural transition as the system's self-activation strength is increased. We note that the self-activation strength parameter (S) is a composite parameter which, after non-dimensionalisation, also scales with the system's input strength. Hence, S can be tuned

by either modifying the self-activation strength or the system input. In the $D \lesssim 1$ region, the model exhibits behaviours dependent on bistability, such as stochastic switching, stable bistability, and heterogeneous activation. Conversely, the $D \gtrsim 1$ region exhibits behaviours related to oscillations and excitability, including stochastic pulsing, oscillations, and stochastic anti-pulsing (Supplementary Section 3.2, Supplementary Figure 4).

Next, by measuring how the prevalence of each behaviour depended on the parameters τ, v_0, n, η, we characterised how these affect the system (Supplementary Figures 10-19). Here, τ (the time delay) was an important determinant for the behaviours in the $D \gtrsim 1$ region (with all behaviours, except for intermediate activation, requiring a longer time delay), with less effect on the $D \lesssim 1$ (which makes sense, since this region has a weak degree of self-deactivation, which is the property τ affects) (Supplementary Figures 10-19). Contrary, v_0 (the base activity of the operon) had only minor effects on the $D \gtrsim 1$ region, while all behaviours in the $D \lesssim 1$ grew less prevalent as v_0 grew larger. Almost all behaviours were affected by η (the degree of system noise), while n (the degree of system ultrasensitivity) had the least pronounced effect on the system's behaviour.

Finally, we note that the response behaviours of σ^V (heterogeneous activation) and σ^B (stochastic pulsing) occur in a distinct part of parameter space, with σ^V in the $D \lesssim 1$ and σ^B in the $D \gtrsim 1$ region. This distinction predicts that varying S will cause the two sigma factors to undergo unique transitions between different behaviours. In the next two sections, we validate these transitions through experimental measurements of the two systems.

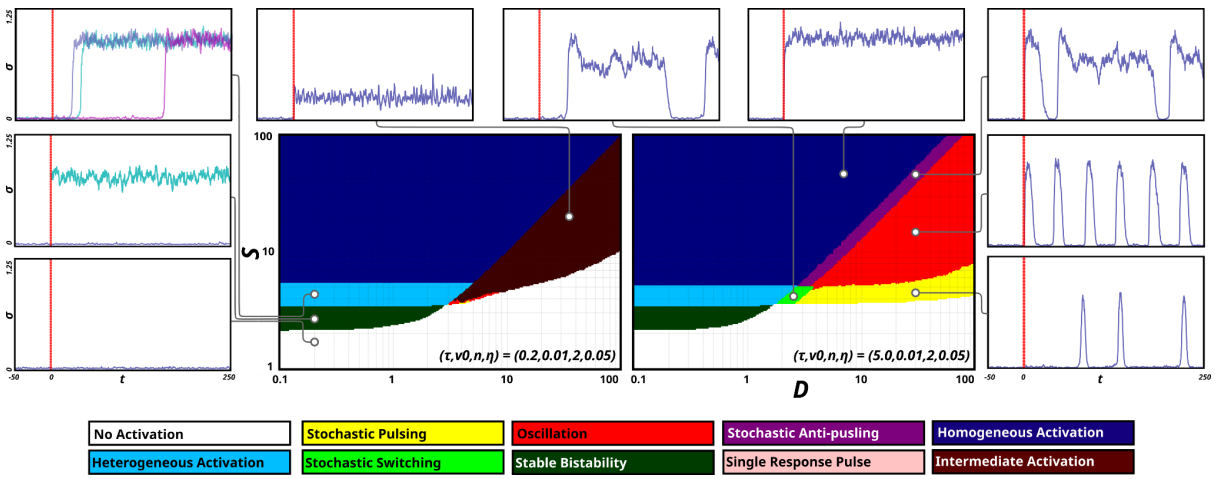

Figure 3. The system's behaviours can be mapped across parameter space. *We apply our behaviour classifier to each point in 6d parameter space. Here we show slices in logarithmic 2d S-D space (where τ, v_0, n, and η are fixed). Trajectories show example simulations from various marked parameter sets, demonstrating how the behaviours change throughout parameter space. We note that the S-D maps change depending on the value of*

the additional parameters. However, its division into a region with bistability-dependant behaviours (for $D \lesssim 1$) and one with pulsing/oscillatory behaviours (for $D \gtrsim 1$) seems to be preserved (and also demonstrated in stability analysis, Supplementary Figure 3). In Supplementary Section 4 we investigate closer how the system's behaviour changes with τ, v_0, n, and η. Additional behaviour maps can be found in Supplementary Figures 5-9.

The bistable behaviour transition predicted by the model is replicated in the σ^V system

We first experimentally tested the transitions predicted for the bistability-dominated $D \lesssim 1$ region, using the *B. subtilis* alternative sigma factor σ^V as a model system. σ^V regulates the lysozyme stress response in *B. subtilis*, activating genes related to cell wall protection and repair (32,33,35,36,51). In a previous study, we documented the behavioural transition of the wild-type system as S is varied (31). In that study, lysozyme stress input was varied, which corresponds to a modulation of S in our simulations. Using single-cell time-lapse microscopy, the study demonstrated a transition from no activation, to heterogeneous activation, to more homogeneous activation, as lysozyme was increased, similar to the transitions observed when S is increased in the $D \lesssim 1$ region of the parameter map (Figure 3). We note that in our model the no activation and heterogeneous activation regions typically (but not always) are separated by a stable bistability region. However, accounting for this behaviour appearing as no activity in these simple input-onset experiments, the experimental results align with our model.

Next, our model predicts that the two regions ($D \lesssim 1$ and $D \gtrsim 1$) can coexist in the same system, and a transition from the former to the latter is possible by increasing D (the degree of system self-deactivation). To test this, we engineered several modified σ^V circuits, where D was artificially increased by adding additional copies of the anti-sigma factor (rsiV) (Methods). When activated by σ^V, RsiV deactivates σ^V's activity (37,38). Here, our model predicts increasing D values will reduce σ^V's activity in the ON state, while the activation remains heterogenous. Finally, for high enough D, all activity should be suppressed (Figure 4B). We tested these predictions using single-cell microscopy in the mother machine microfluidic device. Seven engineered P_{sigV}-*yfp* reporter strains, each containing different copy numbers of *rsiV* (and therefore different D levels), were subjected to 1 µg/mL lysozyme stress. As the copy number of *rsiV* increased, the trend of σ^V ON state activity decreased as expected, while its heterogeneity remained, consistent with the model's predictions. At the highest D levels, σ^V activity was entirely suppressed. These results confirm our model's predictions across the seven engineered strains.

Finally, we consider the σ^V system's transitions in the $D \gtrsim 1$ region. Here, depending on the system's additional four parameters (τ, v_0, n, and η, with τ having the primary effect, Supplementary Section 3.3) the system can exhibit a transition to either pulsing/oscillatory behaviours, or intermediate activation (Figure 3, Supplementary Figures 6-9). To verify in which region of parameter space the system is in, we modulated the *S* value in our two high *D* strains by adding an additional copy of *sigV* driven by its own promoter and by varying lysozyme stress levels. We found that σ^V's transition specifically falls into the intermediate activation category (Figure 4E,F). Finally, the model predicts that in the intermediate transition there is no heterogeneity in activation times. Also, the system's steady state activity level should increase smoothly with increasing *S* levels and decreasing *D* levels (Figure 4E). Again, this prediction is validated by the experiments (Figure 4F).

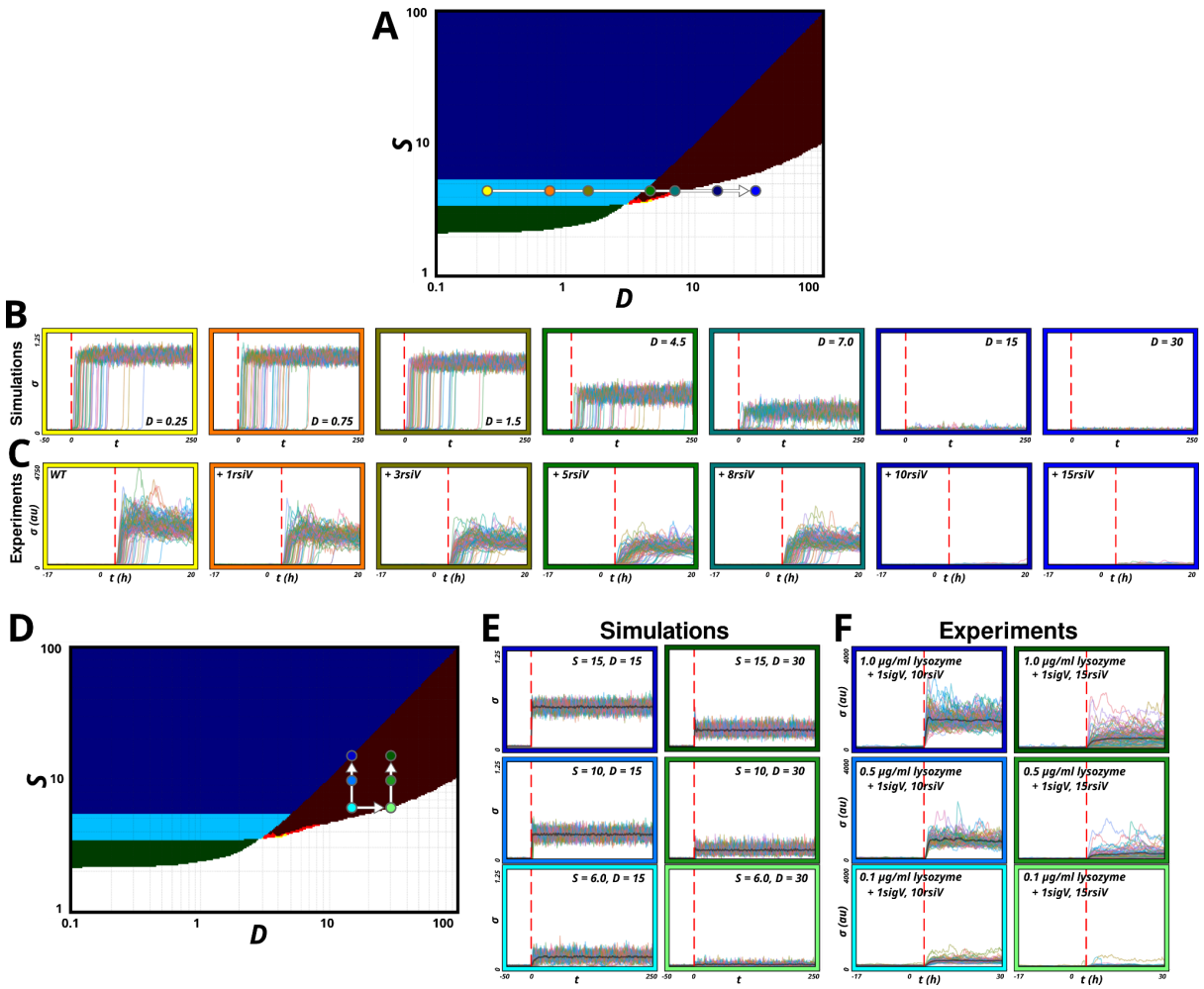

Figure 4. The model's predicted transitions through the heterogeneous and intermediate activation behaviours are validated in the σ^V system. *The wildtype σ^V system has previously been found to undergo a heterogeneous activation transition as S is modulated (31).* ***(A-B)*** *In the model, a system which displays a heterogeneous activation will see the activity level in the ON state reduced as the value of D is increased (with the system transitioning to a no activation behaviour for high enough D values).* ***(A)*** *7 different D values*

shown sampled on a S-D map. ***(B)*** *7 sets of simulation (with n = 50 and D values corresponding to the samples in A).* ***(C)*** *By adding additional σ^V-activated copies of the anti-sigma factor (rsiV) we increase the system's degree of self-deactivation (D value). For 7 different experimental D values experimental measurements are shown. These confirm the decrease in ON state activity with D as predicted by the model.* ***(D-E)*** *A heterogeneous activation system which has been inactivated by increased D levels can be reactivated by further increases to S.* ***(D)*** *6 sampled D and S values from a behaviour map exhibiting intermediate activation.* ***(E)*** *Simulations corresponding to the S,D values in (D). Mean activity (grey lines) increases with S, but is decreased by D.* ***(F)*** *In the experimental system, in a similar manner to C we modulate the value of D by adding additional rsiV copies. The value of S is modulated by increasing the lysozyme input (an additional sigV copy is also added to increase S, permitting us to perform the experiments at lower lysozyme levels). The experiments shows that the system exhibits the intermediate activation transition as it is reactivated by increased S levels. Furthermore, it validates the predictions from (E), where mean activity (grey lines) is increased with S and reduced with D.*

The monounstable behaviour transition predicted by the model is replicated in the σ^B system

Next, we investigated if it is possible to achieve the transitions observed in pulsing/oscillation tuning (via *S*) from Figure 3. For this, we used σ^B, which governs the general stress response in *B. subtilis (52–54)*. Under persistent energy stress, it has previously been shown to exhibit a stochastic pulsing behaviour (8,28). According to our parameter maps, increasing *S* should transition the pulsing dynamics into oscillations. For σ^V we primarily tuned the parameter *S* through the magnitude of the stress input. However, observation of potential high-*S* behaviours (such as oscillations) by tuning energy stress levels is not possible in σ^B, as high energy stress causes secondary effects such as cell death. To avoid this issue, we rewired the σ^B circuit to synthetically drive σ^B via its energy stress pathway. In a *B. subtilis* strain containing a reporter for σ^B activity, P_{sigB} - *yfp*, we first knocked out *rsbP* and *rsbU*, the upstream phosphatases that activate the anti-anti-sigma factor RsbV under stress (Methods). Next, we chromosomally integrated a mutated form of RsbP, which is constitutively active, under the control of an IPTG inducible promoter to drive σ^B expression. The mutated RsbP had the PAS and coiled-coil region removed causing it to be constitutively active (55). This enabled us to vary *S* experimentally (by adding IPTG to the growth medium), investigating the system's response for a range of values.

We scanned our parameter space maps to determine which transition the system undergoes, given it starts in stochastic pulsing (the behaviour found in σ^B), as *S* is modulated (Supplementary Section 3.3). We note that stochastic pulsing is almost exclusively preceded (for lower *S*) by no activation, and proceeded (for higher *S*) by oscillation (Supplementary

Table 1). In addition, for high enough *S*, the system activates homogeneously. Finally, for some systems, the oscillating and the homogeneous activation regions are separated by a region of stochastic anti-pulsing (Figure 5A, Supplementary Figures 6-9).

Next, we measured the σ^B activity of our rewired P_{sigB} - *yfp* strain in the mother machine microfluidics device across various concentrations of IPTG (Methods). As IPTG levels increased from low to high, the σ^B system transitioned through no activation, stochastic pulsing, oscillation, and homogeneous activation behaviours, similar to as predicted by the model (Figure 5B,C). To further validate these findings, we developed a new classifier capable of quantifying the extent to which these four behaviors occur in both model simulations and experimental time trajectories. Unlike the original classifier, which relies on analytical steady-state analysis of parameter values and cannot be applied to experimental data, this new classifier works directly with time-series data. Applying it to both model and experimental data revealed the same transitions (Figure 5B,D). However, we note that the stochastic anti-pulsing behaviour, which appears in the model, is not reproduced experimentally. This discrepancy could be explained by the half-life of the fluorescent marker for σ^B not providing high enough time resolution to distinguish the anti-pulses, or by additional complexity of the σ^B pathway enabling a different transition than what is predicted by our minimal model. Additionally, for some combinations of τ, v_0, n and η, the model also displays the no activation to stochastic pulsing to oscillation to homogeneous activation transition. This transition, however, is much rarer than the one that includes stochastic anti-pulsing (Supplementary Figures 6-9). Finally, the transition predicted by our minimal model, and confirmed by our experiments, are in agreement with a previous stochastic model of the full circuit, which predicted a similar transition (56).

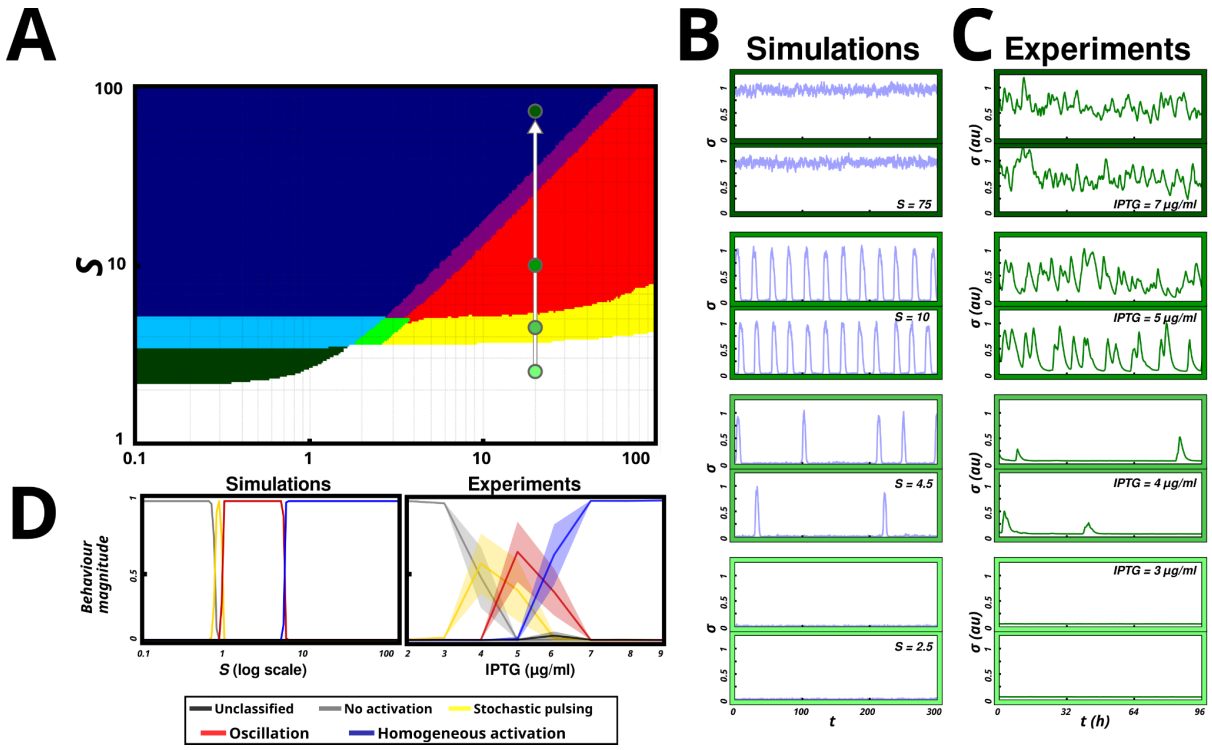

Figure 5. The model's predicted transitions through the stochastic pulsing and oscillation behaviours are validated in the σ^B system. (A) *A behaviour map which, in its D≳1 region, exhibits a stochastic pulsing/oscillation transition with S.* ***(B)*** *Sample simulation trajectories (under constant and active input) are shown for 4 different S levels (each set of two simulations are performed at the corresponding parameter sets marked with coloured dots in A).* ***(C)*** *Example traces of the rewired* P_{sigB} *- yfp strain (Methods) for 4 different IPTG levels. The no activation -> stochastic pulsing -> oscillation -> homogeneous activation transition predicted by the simulations is confirmed in the experiments.* ***(D)*** *We created a classifier capable of classifying both simulated and experimental trajectories as either no activation, stochastic pulsing, oscillation, or homogeneous activation. When applying it to our simulations (taken from the transition marked in A) and experimental measurements (at IPTG levels ranging from 2μg/ml to 9 μg/ml) we see similar transitions. Shaded regions denote standard deviation over 5 repeats of experiments.*

Discussion

In this work, we present a general model of a mixed positive/negative feedback loop, through which we describe ten distinct dynamic behaviours that this circuit is capable of producing. By employing an automated classification scheme, we mapped the occurrence of these

behaviours across parameter space, revealing how each behaviour depends on the system's properties (parameters). We applied our model to bacterial sigma factors, whose circuits contain mixed positive/negative feedback loops. For systems with well-characterized behaviours, our model predicts their properties. For example, the σ^B circuit, known for its stochastic pulsing behaviour, is predicted to exhibit a higher degree of self-deactivation (*D*) compared to the σ^V system, which displays heterogeneous activation. Conversely, the model also predicts how changes in system properties influence behaviours. A more thorough analysis (than what is presented in the paper) of each behaviour's dependency on each parameter is provided in the supplementary material (Supplementary Section 4).

We divide parameter space into two approximate regions, $D \lesssim 1$ and $D \gtrsim 1$, each undergoing a distinct behaviour transition as *S* is varied. For $D \lesssim 1$ the system undergoes a bistable transition, while for $D \gtrsim 1$ a range of pulsing and oscillatory behaviours are exhibited. This means that each region undergoes a unique set of behaviours as the input parameter (*S*) is varied. To validate our model, we examined the behaviours of two real systems (the alternative sigma factors σ^V and σ^B, both from *B. subtilis*) as *S* is increased from small to large. Here, both systems undergo the predicted transition. Furthermore, we showed that by increasing the value of *D*, a system in the $D \lesssim 1$ region (e.g σ^V) can be induced to produce $D \gtrsim 1$-type behaviours. This shows that these two regions, as predicted by the model, can coexist in the same system.

The mixed positive/negative feedback loop is a common motif in cellular pathways. Our general model of this motif provides a comprehensive framework for understanding how these systems generate a wide range of behaviours. It shows how a relatively small and intuitive set of properties determines the specific behaviour produced. Specifically for bacterial sigma factors, several behaviours predicted by our model, including single response pulse, stochastic pulsing, and heterogeneous activation, have been observed using single-cell microscopy (29–31,57). We demonstrate that these behaviours can arise from the core mixed positive/negative feedback loop inherent in these systems. As more sigma factor systems are explored, our model suggests that additional predicted behaviours may also be observed.

Our insights are also relevant to synthetic biology, where mixed positive/negative feedback loops, such as those involving sigma factor circuits, have been proposed as potential regulators of synthetic systems (58–60). Here, we have only experimentally tuned two (*S* and *D*) of the six parameters. Furthermore, the large number of additional genes required to tune *D* makes our approach impractical for most applications. In the future, it will be

important to explore whether synthetic mixed positive/negative feedback loops that allow for tuning additional properties can be developed. The general principles developed here will be invaluable for designing such synthetic regulators with tailored response behaviours.

Materials and Methods

Mathematical model

Our minimal model of a general mixed positive/negative feedback loop tracks the concentration of a single component (σ). Degradation/dilution was assumed to be linear. To make production as general as possible, it was modelled as a Hill function. We note that the model is based on the following three assumptions:

- σ activates its own production.
- σ deactivates its own production.
- The deactivation is subject to a time delay.

To take these into account, production depended on both an activating term (σ) and a repressing term (σ subject to a time delay).

The time delay was implemented using the linear chain trick (LCT) (50,61). While this introduces additional variables to the system, it has the advantage that the model can be represented as ODEs and SDEs (instead of DDEs and SDDEs). After confirming that the number of intermediaries used in the LCT had little effect on the model, we decided to implement it using three intermediaries (Supplementary Figure 1, Supplementary Section 1.2). Finally, we also confirmed that all ten response behaviours could be recreated in a model with a discrete delay (Supplementary Figure 20, Supplementary Section 5.2).

Initially, our model depended on 9 parameters. Since we only sought to investigate qualitative behaviours, nondimensionalisation was performed. This section will describe the nondimensionalised model. The nondimensionalisation process and the non-nodimensionalised model are described in Supplementary Section 1.1.

Reactions

Initially, our model contains only two reactions, production and degradation (or dilution) of the sigma factor (σ, the CRN's only species). An additional three production and degradation reactions are added by the LCT (which also adds three intermediary species, A_1, A_2, and A_3). These reactions are described in Table 1.

Description	Reaction	Rate	Propensity
Production	∅ —> σ	V_0 + $(S[\sigma])^n/((S[\sigma])^n+(D[A_3])^n+1)$	V_0 + $(S[\sigma])^n/((S[\sigma])^n+(D[A_3])^n+1)$
Degradation/dilution	σ —> ∅	1	$[\sigma]$
Production (LCT)	∅ —> A_1	$[\sigma]/\tau$	$[\sigma]/\tau$
	∅ —> A_2	$[A_1]/\tau$	$[A_1]/\tau$
	∅ —> A_3	$[A_2]/\tau$	$[A_2]/\tau$
Degradation/dilution (LCT)	A_1 —> ∅	$1/\tau$	$[A_1]/\tau$
	A_2 —> ∅	$1/\tau$	$[A_2]/\tau$
	A_3 —> ∅	$1/\tau$	$[A_3]/\tau$

Table 1: *The reactions of the general sigma factor circuit model. The model primarily consists of two reactions, production and degradation of the sigma factor (σ). However, since the time delay (of the negative feedback of σ on its own production) is implemented using the LCT, an additional 3 species (*A_1, A_2, and A_3*) are introduced. This also adds an additional three production and three degradation reactions.*

Parameters

Our nondimensionalised model consists of 6 parameters, as described in Table 2. The model does not have specific parameter values. Instead, every instance of the model, with specific values of (S,D,τ,v_0,n,η) represents a potential mixed positive/negative feedback loop. E.g. by letting S be large and D small, we can investigate the behaviour of circuits with high degrees of self-activation and low degrees of self-deactivation. As we scan these parameters' values we can investigate how systems' properties affect their behaviours. These scans are made possible through the nondimensionalisation process, which limits the dimension of parameter space.

Parameter	Description
S	Degree of self-activation (also includes input strength).
D	Degree of self-deactivation.
τ	Length of the self-deactivation time delay.
v_0	Operon base activity/leakage.
n	Hill coefficient (degree of non-linearity in the circuit).

η	Degree of noise in the circuit.

Table 2: *The parameters of the (non-dimensionalised) general sigma factor model.*

We note that the parameter S is a composite of the pre-nondimensionalised parameters $\hat{S}$ and $\hat{I}$, where $\hat{S}$ is the degree of system self-activation, and $\hat{I}$ the magnitude of the input signal (Supplementary Section 1.1). Hence, modulation to a system's input corresponds to modulation of the parameter S.

Model Simulations

We wish to investigate the model's behaviour in response to an input. In the absence of the input (in response to which we wish to investigate the response), $S=0$. When we simulate our model for a specific parameter set (S,D,τ,v_0,n,η), we will initialise it with $S=0$, with the parameter S only attaining its designated value at the time of input onset (always at time $t=0$). E.g. a model instance may be defined by the parameter set $(S,D,\tau,v_0,n,\eta)=(5.0,5.0,10.0,0.1,2,0.1)$, and simulated throughout the time interval $(-500,2000)$. The simulations start with the parameter values $(0.0,5.0,10.0,0.1,2,0.1)$, which are changed to $(5.0,5.0,10.0,0.1,2,0.1)$ at time 0, at which point the system activates.

It would be possible to vary the value of S throughout a simulation, to model inputs with varying magnitude. However, for simplicity, this work will only consider systems with a step increase in the input.

Practically, the model was implemented using in the Julia programming language using the Catalyst.jl modelling package (62). All simulations were carried out using the DifferentialEquations.jl package (63). The ImplicitEM solver was used as it handles stiff SDE systems well, and allows for adaptive time stepping (64). Gillespie simulations were simulated using the JumpProcesses.jl package (65).

Automated behaviour classification

Initial steady state and stability analysis of our model determined that it may have either 0, 1, or 2 stable steady states (Supplementary Section 2.1). While a dynamic system asymptotically approaches a stable steady state, perturbations may cause a transition towards another steady state. Such perturbations may either be transient (change in input magnitude) or asymptotic (noise). Based on the possible transitions between the system's potential steady states, we designed a classification scheme for the system's behaviour

(Supplementary Section 6.1). This scheme takes into account the possibility of excitable and oscillatory behaviours. A total of 10 system behaviours (as described in the Results) were predicted. Further behaviours could be created by subdividing the initial ten, however, we deemed such subdivisions non-beneficial (Supplementary Section 6.1). Further description and analysis of the individual behaviours can be found in Supplementary Section 4.

To enable our mapping of behaviour across parameter space, we created a decision tree-based heuristic classifier algorithm. When provided a parameter set (S,D,τ,v_0,n,η), the algorithm simulates the model multiple times, and assigns it one of the behavioural classes described in Figure 2. The full algorithm is described in Supplementary Section 6. In addition, to further prove its validity, we randomly generated 10 parameter sets from each behaviour (as classified by the algorithm). By showing that simulations of these parameter sets align with their designated behaviours, we demonstrate the efficacy of the algorithm (Supplementary Section 6.3).

Experiments

Strains and Media

All strains are derived from *B. subtilis* 168 or PY79. Deletions were made by recombination of linear DNA fragments homologous to the region of interest and replacing the gene of interest with an antibiotic resistance cassette. All strains had a housekeeping σ^A promoter-driven mCherry as a constitutive control and for segmentation.

Cells were grown in Spizizen's Minimal Media (SMM) (66). It contained 50 µg/ml Tryptophan as an amino acid source and 0.5% glucose as a carbon source. Cultures were started from frozen stock in SMM and grown overnight at 30°C to an OD between 0.3 and 0.8. The overnight cultures were resuspended to an OD of 0.01 and regrown to an OD of 0.1 at 37°C.

Plasmids

E. coli strain DH5α was used to clone all plasmids. The cloning was done with a combination of standard molecular cloning techniques using Clonetech In-Fusion Advantage PCR Cloning kits and non-ligase dependent cloning. Plasmids were chromosomally integrated into the 168 or PY79 background via double crossover using standard techniques. The list below provides a description of the used plasmids, with details on selection marker and integration position/cassette given at the beginning. Note that all plasmids below replicate in *E. coli* but not in *B. subtilis.*

.

1. **ppsB::P_{trpE} - *mCherry* ErmR**

   This plasmid was used to provide uniform expression of mCherry from a σ^A-dependent promoter, enabling automatic image segmentation (cell identification) in time-lapse movie analysis. A minimal σ^A promoter from the *trpE* gene was cloned into a vector with *ppsB* homology regions (28). The original integration vector was a gift from A. Eldar (67).

2. **sacA::P_{sigB} - *yfp* CmR**

   The target promoter of *sigB* was cloned into the EcoRI/BamHI sites of AEC127 (67) yielding a Venus (YFP) reporter for σ^B activity (gift from M. Elowtiz, CalTech).

3. **amyE::$P_{hyperspank}$ - *rsbP*Δ4 (ΔPAS-CC)**

   The coding region of a *rsbP* mutant lacking PAS and the coiled-coil region along with a 5' transcriptional terminator, was cloned downstream of the hyperspank IPTG-inducible promoter in plasmid pDR-111 (gift from D. Rudner, Harvard). *rsbP*Δ4 (ΔPAS-CC) is described in (55).

4. ***sacA*::P_{sigV} -*yfp* CmR**

   The target promoter of *sigV* was cloned into the EcoRI/BamHI sites of AEC12 (Eldar *et al,* 2009) (gift from M. Elowitz, CalTech).

5. ***amyE*::P_{sigV}-? x *rsiV* SpecR**

   The target promoter of *sigV* with multiple copies of *rsiV* (?= 1x, 3x, 5 x) were cloned into the sites EcoRI/BAmHI and BamHI/HindIII of pdL30 (Locke et al, 2011).

6. ***lacA*::P_{sigV} - 5 x *rsiV* TetR**

   The target promoter of *sigV* with five copies of *rsiV* was cloned into the sites EcorI/Nde of a variation of ECE174 (gift from M. Elowitz, CalTech).

7. ***pyrD*::P_{sigV} - 5 x *rsiV* NatR**

   The target promoter of *sigV* with five copies of *rsiV* was cloned into the sites EcoRI/BAmHI of a variation of ECE174 (gift from M. Elowitz, CalTech).

8. ***hag*::P_{sigV} - *sigV* ErmR**

   The target promoter of *sigV* driving *sigV* and 400 upstream and downstream homology regions of hag was cloned into EcorV of pBS II SK (-)

Strain List

Strain Name	Genotype	Source
PY79	BGSC 1A747	BGSC
PB2	168 (trpC2)	BGSC
JP1/JLB54	PY79 *ppsb*::P_{trpE} - *mCherry* (Phleo^R)	(8)
JP2	JP1; *ytvA*::*neo*	(8)
JLB047	JP2; *sacA*::P_{sigV} - *yfp* (Cm^R)	(31)
JLB130	JLB047; *hag*::ErmR	(31)
JLB212	JLB130; *amyE*::P_{sigV} - *rsiV* SpecR	(31)
JLB288	JLB130; *amyE*::3x P_{sigV} - *rsiV* SpecR	This work
JLB293	JLB130; *amyE*::5x P_{sigV} - *rsiV* SpecR	This work
JLB297	JLB288; *lacA*::5x P_{sigV} - *rsiV* TetR	This work
JLB325	JLB293; *lacA*::5x P_{sigV} - *rsiV* TetR	This work
JLB324	JLB325; *pyrD*::5x P_{sigV} - *rsiV* NatR	This work
JLB327	JLB47; *lacA*::5x P_{sigV} - *rsiV* TetR *amyE*::5x P_{sigV} - *rsiV* SpecR *hag*:: P_{sigV} - *sigV* ErmR	This work
JLB82	JLB47; *amyE*::5x P_{sigV} - *rsiV* SpecR *lacA*::5x P_{sigV} - *rsiV* TetR *pyrD*::5x P_{sigV} - *rsiV* NatR *hag*::P_{sigV} - *sigV* ErmR	This work
JJB176	PB2; *ppsb*::P_{trpE} - *mCherry* Phleo R	(28)
JJB213	JJB176; *sacA*::P_{sigB} - *yfp* CmR	(28)
JJB240	JJB213; *rsbU*::KanR	(28)
JJB441	JJB241; *amyE*::$P_{hyperspank}$ - *rsbP*Δ4 (ΔPAS-CC) SpecR	This work
JLB264	JJB441; *rsbQP*::TetR	This work
JLB265	JLB264; *hag*::ErmR	This work

Table 3: *List of strains used in this article.*

Microscopy

An inverted Nikon Ti-E microscope (Nikon, Netherlands) with a Photometrics Prime sCMOS camera (Photometrics, USA) and a 100x phase Plan Apo (NA 1.4) objective (Nikon, Netherlands) were used for all experiments. Brightfield illumination was provided by a LED lamp (CoolLED, UK) and for Epifluorescence illumination a Lumencore Solar II light engine (Lumencore USA) was used. Chroma filters (Chroma, Bellows Falls, USA) #41027 for the RFP channel and #49003 for the YFP channel were used in combination with the epifluorescence. For temperature control a stage incubator (Solent Scientific, UK) was set at 37°C for all experiments. Metamorph (Molecular Device, Sunnyvale, CA, USA) controlled the camera, the motorised stage (Nikon, Amsterdam, Netherlands) and the microscope.

Microfluidic Designs

Two microfluidic designs were used in this study. All experiments on σ^B were done in a traditional mother machine device (26). The master for these chips was fabricated by exploiting a Kloe Dilase 650, direct laser writer (Kloe, France). More details on the fabrication can be found in the supplementary information. All experiments on σ^V were done in a mother machine device with side trenches (68). This epoxy master was a kind gift from the Ellowitz lab.

Microfluidic Chip fabrication

All microfluidics chips were made using Sylgard 184 polydimethylsiloxane (PDMS) (Dow Corning, USA) using a 10:1 base to curing agent ratio. The PDMS was poured onto the silicon master and cured at 65C for 2h. Chips were cut out and inlets were punched into the PDMS using a 1 mm biopsy puncher (WPI, UK). The chips were then plasma bonded to glass bottom dishes (Wilco Wells, Netherlands) using a Femto Plasma System (Diener, Germany) (12s at 30W and 0.35 mbar). To strengthen the bonding of the PDMS to the glass dish the chips were put into the oven for 10 min at 65°C.

Microfluidic Experiments

10 ml of the regrown overnight culture with an of OD 0.1 were spun down at 4000 rpm (3000 g) for 10 min and resuspended in 100 µl. This cell suspension was loaded into the feeding channels and spun for 5 min at 3000 rpm using a spin coater (Polos SPIN150i, SPS) to improve the loading of the cells into the growth channels.

The loaded chips were then mounted onto the microscope stage and connected to a syringe

pump (KD Scientific, USA) using tygon tubing (Cole Parmer, USA). A constant flow rate of 0.15 ml/h and a temperature of 37°C was maintained throughout the experiment.

All movies were analysed using a modified version of the Schnitzcells package (69) for MATLAB (Mathworks, USA) optimised for mother machine experiments.

Bibliography

1. Xiong W, Ferrell JE. A positive-feedback-based bistable “memory module” that governs a cell fate decision. Nature. 2003 Nov 27;426(6965):460–5.
2. Umulis DM, Serpe M, O’Connor MB, Othmer HG. Robust, bistable patterning of the dorsal surface of the Drosophila embryo. Proc Natl Acad Sci USA. 2006 Aug 1;103(31):11613–8.
3. Goldbeter A. A minimal cascade model for the mitotic oscillator involving cyclin and cdc2 kinase. Proc Natl Acad Sci USA. 1991 Oct 15;88(20):9107–11.
4. Elowitz MB, Leibler S. A synthetic oscillatory network of transcriptional regulators. Nature. 2000 Jan 20;403(6767):335–8.
5. Hubaud A, Regev I, Mahadevan L, Pourquié O. Excitable Dynamics and Yap-Dependent Mechanical Cues Drive the Segmentation Clock. Cell. 2017 Oct 19;171(3):668-682.e11.
6. Süel GM, Garcia-Ojalvo J, Liberman LM, Elowitz MB. An excitable gene regulatory circuit induces transient cellular differentiation. Nature. 2006 Mar 23;440(7083):545–50.
7. Briat C, Gupta A, Khammash M. Antithetic integral feedback ensures robust perfect adaptation in noisy biomolecular networks. Cell Syst. 2016 Jan 27;2(1):15–26.
8. Park J, Dies M, Lin Y, Hormoz S, Smith-Unna SE, Quinodoz S, et al. Molecular Time Sharing through Dynamic Pulsing in Single Cells. Cell Syst. 2018 Feb 28;6(2):216-229.e15.
9. Arkin A, Ross J, McAdams HH. Stochastic kinetic analysis of developmental pathway bifurcation in phage lambda-infected Escherichia coli cells. Genetics. 1998 Aug;149(4):1633–48.
10. Gillespie DT. Stochastic simulation of chemical kinetics. Annu Rev Phys Chem. 2007;58:35–55.
11. Paranjpe DA, Sharma VK. Evolution of temporal order in living organisms. J Circadian Rhythms. 2005 May 4;3(1):7.
12. Lee B, Shin D, Gross SP, Cho K-H. Combined Positive and Negative Feedback Allows Modulation of Neuronal Oscillation Frequency during Sensory Processing. Cell Rep. 2018 Nov 6;25(6):1548-1560.e3.
13. Mugler A, Kittisopikul M, Hayden L, Liu J, Wiggins CH, Süel GM, et al. Noise Expands the Response Range of the Bacillus subtilis Competence Circuit. PLoS Comput Biol. 2016 Mar 22;12(3):e1004793.

14. Pomerening JR, Kim SY, Ferrell JE. Systems-level dissection of the cell-cycle oscillator: bypassing positive feedback produces damped oscillations. Cell. 2005 Aug 26;122(4):565–78.

15. Devany E, Zhang X, Park JY, Tian B, Kleiman FE. Positive and negative feedback loops in the p53 and mRNA 3' processing pathways. Proc Natl Acad Sci USA. 2013 Feb 26;110(9):3351–6.

16. Barkai N, Leibler S. Circadian clocks limited by noise. Nature. 2000 Jan 20;403(6767):267–8.

17. Vilar JMG, Kueh HY, Barkai N, Leibler S. Mechanisms of noise-resistance in genetic oscillators. Proc Natl Acad Sci USA. 2002 Apr 30;99(9):5988–92.

18. Stricker J, Cookson S, Bennett MR, Mather WH, Tsimring LS, Hasty J. A fast, robust and tunable synthetic gene oscillator. Nature. 2008 Nov 27;456(7221):516–9.

19. Afroz T, Beisel CL. Understanding and exploiting feedback in synthetic biology. Chem Eng Sci. 2013 Nov;103:79–90.

20. Himmelreich R, Hilbert H, Plagens H, Pirkl E, Li BC, Herrmann R. Complete sequence analysis of the genome of the bacterium Mycoplasma pneumoniae. Nucleic Acids Res. 1996 Nov 15;24(22):4420–49.

21. Gruber TM, Gross CA. Multiple sigma subunits and the partitioning of bacterial transcription space. Annu Rev Microbiol. 2003;57:441–66.

22. Cook H, Ussery DW. Sigma factors in a thousand E. coli genomes. Environ Microbiol. 2013 Dec;15(12):3121–9.

23. Helmann JD. Anti-sigma factors. Curr Opin Microbiol. 1999 Apr;2(2):135–41.

24. Paget MS. Bacterial Sigma Factors and Anti-Sigma Factors: Structure, Function and Distribution. Biomolecules. 2015 Jun 26;5(3):1245–65.

25. Davis MC, Kesthely CA, Franklin EA, MacLellan SR. The essential activities of the bacterial sigma factor. Can J Microbiol. 2017 Feb;63(2):89–99.

26. Wang P, Robert L, Pelletier J, Dang WL, Taddei F, Wright A, et al. Robust growth of Escherichia coli. Curr Biol. 2010 Jun 22;20(12):1099–103.

27. Hamm CW, Butler DR, Cabeen MT. Bacillus subtilis Stressosome Sensor Protein Sequences Govern the Ability To Distinguish among Environmental Stressors and Elicit Different σB Response Profiles. MBio. 2022 Dec 20;13(6):e0200122.

28. Locke JCW, Young JW, Fontes M, Hernández Jiménez MJ, Elowitz MB. Stochastic pulse regulation in bacterial stress response. Science. 2011 Oct 21;334(6054):366–9.

29. Patange O, Schwall C, Jones M, Villava C, Griffith DA, Phillips A, et al. Escherichia coli can survive stress by noisy growth modulation. Nat Commun. 2018 Dec 17;9(1):5333.

30. Young JW, Locke JCW, Elowitz MB. Rate of environmental change determines stress response specificity. Proc Natl Acad Sci USA. 2013 Mar 5;110(10):4140–5.

31. Schwall CP, Loman TE, Martins BMC, Cortijo S, Villava C, Kusmartsev V, et al. Tunable phenotypic variability through an autoregulatory alternative sigma factor circuit. Mol Syst Biol. 2021 Jul;17(7):e9832.

32. Guariglia-Oropeza V, Helmann JD. Bacillus subtilis σ(V) confers lysozyme resistance

by activation of two cell wall modification pathways, peptidoglycan O-acetylation and D-alanylation of teichoic acids. J Bacteriol. 2011 Nov;193(22):6223–32.

33. Ho TD, Hastie JL, Intile PJ, Ellermeier CD. The Bacillus subtilis extracytoplasmic function σ factor σ(V) is induced by lysozyme and provides resistance to lysozyme. J Bacteriol. 2011 Nov;193(22):6215–22.

34. Ho TD, Ellermeier CD. Extra cytoplasmic function σ factor activation. Curr Opin Microbiol. 2012 Apr;15(2):182–8.

35. Hastie JL, Williams KB, Sepúlveda C, Houtman JC, Forest KT, Ellermeier CD. Evidence of a bacterial receptor for lysozyme: binding of lysozyme to the anti-σ factor RsiV controls activation of the ecf σ factor σV. PLoS Genet. 2014 Oct 2;10(10):e1004643.

36. Hastie JL, Williams KB, Bohr LL, Houtman JC, Gakhar L, Ellermeier CD. The Anti-sigma Factor RsiV Is a Bacterial Receptor for Lysozyme: Co-crystal Structure Determination and Demonstration That Binding of Lysozyme to RsiV Is Required for σV Activation. PLoS Genet. 2016 Sep 7;12(9):e1006287.

37. Castro AN, Lewerke LT, Hastie JL, Ellermeier CD. Signal Peptidase Is Necessary and Sufficient for Site 1 Cleavage of RsiV in Bacillus subtilis in Response to Lysozyme. J Bacteriol. 2018 Jun 1;200(11):e00663-17.

38. Lewerke LT, Kies PJ, Müh U, Ellermeier CD. Bacterial sensing: A putative amphipathic helix in RsiV is the switch for activating σV in response to lysozyme. PLoS Genet. 2018 Jul 18;14(7):e1007527.

39. Benson AK, Haldenwang WG. Characterization of a regulatory network that controls sigma B expression in Bacillus subtilis. J Bacteriol. 1992 Feb;174(3):749–57.

40. Dufour A, Haldenwang WG. Interactions between a Bacillus subtilis anti-sigma factor (RsbW) and its antagonist (RsbV). J Bacteriol. 1994 Apr;176(7):1813–20.

41. Alper S, Dufour A, Garsin DA, Duncan L, Losick R. Role of adenosine nucleotides in the regulation of a stress-response transcription factor in Bacillus subtilis. J Mol Biol. 1996 Jul 12;260(2):165–77.

42. Wise AA, Price CW. Four additional genes in the sigB operon of Bacillus subtilis that control activity of the general stress factor sigma B in response to environmental signals. J Bacteriol. 1995 Jan;177(1):123–33.

43. Kalman S, Duncan ML, Thomas SM, Price CW. Similar organization of the sigB and spoIIA operons encoding alternate sigma factors of Bacillus subtilis RNA polymerase. J Bacteriol. 1990 Oct;172(10):5575–85.

44. Cabeen MT, Russell JR, Paulsson J, Losick R. Use of a microfluidic platform to uncover basic features of energy and environmental stress responses in individual cells of Bacillus subtilis. PLoS Genet. 2017 Jul 20;13(7):e1006901.

45. Voelker U, Voelker A, Haldenwang WG. Reactivation of the Bacillus subtilis anti-sigma B antagonist, RsbV, by stress- or starvation-induced phosphatase activities. J Bacteriol. 1996 Sep;178(18):5456–63.

46. Chen C-C, Yudkin MD, Delumeau O. Phosphorylation and RsbX-dependent dephosphorylation of RsbR in the RsbR-RsbS complex of Bacillus subtilis. J Bacteriol.

2004 Oct;186(20):6830–6.

47. Gillespie DT. The chemical Langevin equation. Journal of Chemical Physics. 2000;113(1):297–306.

48. Wilkinson DJ. Stochastic modelling for quantitative description of heterogeneous biological systems. Nat Rev Genet. 2009 Feb;10(2):122–33.

49. Metz J, Diekmann 0. Exact Finite Dimensional Representations of Models for Physiologically Structured Populations.I: The Abstract Foundations of linear Chain Trickery. Differential Equations with Applications in biology, Physics and Engineering, Letcure Notes in Pure & Applied Mathematics. 1991. p. 269–89.

50. MacDonald N. Time lags in biological models. Berlin, Heidelberg: Springer Berlin Heidelberg; 1978.

51. Ho TD, Ellermeier CD. Activation of the extracytoplasmic function σ factor σv by lysozyme. Mol Microbiol. 2019 Jul 9;112(2):410–9.

52. Rodriguez Ayala F, Bartolini M, Grau R. The Stress-Responsive Alternative Sigma Factor SigB of Bacillus subtilis and Its Relatives: An Old Friend With New Functions. Front Microbiol. 2020 Sep 15;11:1761.

53. Haldenwang WG, Losick R. A modified RNA polymerase transcribes a cloned gene under sporulation control in Bacillus subtilis. Nature. 1979 Nov 15;282(5736):256–60.

54. Hecker M, Pané-Farré J, Völker U. SigB-dependent general stress response in Bacillus subtilis and related gram-positive bacteria. Annu Rev Microbiol. 2007;61:215–36.

55. Brody MS, Stewart V, Price CW. Bypass suppression analysis maps the signalling pathway within a multidomain protein: the RsbP energy stress phosphatase 2C from Bacillus subtilis. Mol Microbiol. 2009 Jun;72(5):1221–34.

56. Loman TE, Locke JCW. The σB alternative sigma factor circuit modulates noise to generate different types of pulsing dynamics. PLoS Comput Biol. 2023 Aug 4;19(8):e1011265.

57. Yelleswarapu M, van der Linden AJ, van Sluijs B, Pieters PA, Dubuc E, de Greef TFA, et al. Sigma Factor-Mediated Tuning of Bacterial Cell-Free Synthetic Genetic Oscillators. ACS Synth Biol. 2018 Dec 21;7(12):2879–87.

58. Rhodius VA, Segall-Shapiro TH, Sharon BD, Ghodasara A, Orlova E, Tabakh H, et al. Design of orthogonal genetic switches based on a crosstalk map of σs, anti-σs, and promoters. Mol Syst Biol. 2013 Oct 29;9:702.

59. Bervoets I, Van Brempt M, Van Nerom K, Van Hove B, Maertens J, De Mey M, et al. A sigma factor toolbox for orthogonal gene expression in Escherichia coli. Nucleic Acids Res. 2018 Feb 28;46(4):2133–44.

60. Pinto D, Vecchione S, Wu H, Mauri M, Mascher T, Fritz G. Engineering orthogonal synthetic timer circuits based on extracytoplasmic function σ factors. Nucleic Acids Res. 2018 Aug 21;46(14):7450–64.

61. Metz J, Diekmann O. Exact finite dimensional representations of models for physiologically structured populations.i. In: Goldstein J, editor. Differential Equations with Applications in Biology, Physics, and Enqineering. CRC Press Taylor & Francis

Group 6000 Broken Sound Parkway NW, Suite 300 Boca Raton, FL 33487-2742: CRC Press; 2017. p. 269–90.

62. Loman TE, Ma Y, Ilin V, Gowda S, Korsbo N, Yewale N, et al. Catalyst: Fast and flexible modeling of reaction networks. PLoS Comput Biol. 2023 Oct 18;19(10):e1011530.

63. Rackauckas C, Nie Q. DifferentialEquations.jl – A Performant and Feature-Rich Ecosystem for Solving Differential Equations in Julia. J Open Res Softw. 2017 May 25;5.

64. Rackauckas C, Nie Q. Adaptive methods for stochastic differential equations via natural embeddings and rejection sampling with memory. Discrete Continuous Dyn Syst Ser B. 2017;22(7):2731–61.

65. Zagatti G, Isaacson S, Rackauckas C, Ilin V, Ng S-K, Bressan S. Extending JumpProcesses.jl for fast point process simulation with time-varying intensities. JCON. 2024 Apr 23;6(58):133.

66. Spizizen J. Transformation of biochemically deficient strains of bacillus subtilis by deoxyribonucleate. Proc Natl Acad Sci USA. 1958 Oct 15;44(10):1072–8.

67. Eldar A, Chary VK, Xenopoulos P, Fontes ME, Losón OC, Dworkin J, et al. Partial penetrance facilitates developmental evolution in bacteria. Nature. 2009 Jul 23;460(7254):510–4.

68. Norman TM, Lord ND, Paulsson J, Losick R. Memory and modularity in cell-fate decision making. Nature. 2013 Nov 28;503(7477):481–6.

69. Young JW, Locke JCW, Altinok A, Rosenfeld N, Bacarian T, Swain PS, et al. Measuring single-cell gene expression dynamics in bacteria using fluorescence time-lapse microscopy. Nat Protoc. 2011 Dec 15;7(1):80–8.